Docket No.: PST-29202/36
(PATENT)

IN THE UNITED STATES PATENT AND TRADEMARK OFFICE

In re Patent Application of:
Ali Kaan Kalkan et al.

Application No.: 10/542,951 | Confirmation No.: 2017

Filed: July 21, 2005 | Art Unit: 1794

For: NANOPARTICLE COATED NANOSTRUCTURED SURFACES FOR DETECTION, CATALYSIS AND DEVICE APPLICATIONS | Examiner: J. C. Langman

DECLARATION OF ALI KAAN KALKAN UNDER 37 CFR 1.132

I, Ali Kaan Kalkan, declare as follows:

1. I am assistant professor at the School of Mechanical and Aerospace Engineering at Oklahoma State University.

2. I earned my PhD degree from The Pennsylvania State University in **2001**. From 2001 to 2006 I held a Research Faculty position in Engineering Science at The Pennsylvania State University. In 2003, I co-founded NanoHorizons, Inc., which currently has 25 employees. I am the inventor or co-inventor of 12 US Patents, which have been licensed to six companies. My research in the field of nanostructured materials has resulted in more than thirty publications, several conference awards, and has been recognized on journal covers. I am also the recipient of 2008 Oak Ridge Associated Universities Ralph E. Powe Young Faculty Enhancement Award and 2008 Big 12 Faculty Fellowship.

3. I am a co-inventor on the above-identified patent application, U.S. Patent Application Serial No. 10/542,951 ("the application"). I have read the Office Action issued in

the application dated October 28, 2009 ("the Office Action"). I have also reviewed and am familiar with cited references referred to in the Office Action as Filas et al., Debe, Sun et al., and Zhang et al.

4. Based upon my reading of the Office Action, I understand that pending claims 105 and 107-110 are considered to not be adequately shown within the application with respect to a metal nanocrystal bridging the tops of two adjacent nanostructure columns of the array. In this regard, I refer to attached micrograph that was annotated to become the 90 second panel of Figure 6. I note in the lower left-hand region of the micrograph corresponding to the foreground based on the imaging angle, for example a particle that is approximately 80 nanometers within the plane of the image page. As the nanostructured array on which it lies has columns with an average linear dimension of 20 nanometers and a spatial separation of on average 20 nanometers, then an 80 nanometer silver particle regardless of whether spherical, prolate, oblong or like shape interpreted from this image, must necessarily overlie at least two nanostructured columns. As reductive silver nanoparticle growth in this image is initiated at the nanostructure surface, I interpret this image as the larger metallic nanocrystals being in physical contact with the underlying nanostructured columns. With continued residence time of such a substrate in contact with metal ion solutions, I believe it is apparent from the application and experiments associated with this invention that even larger particles than those shown in the application micrographs are grown across the tops of adjacent nanostructured columns. In contrast, the size of metallic nanocrystals conductively grown in voids between nanostructured columns is limited by void dimensions.

5. I understand that claims 99 and 102-104 are considered to either be anticipated by, or in the alternative be obvious over Filas et al. on the basis that the nanoscale metal particles

of Filas et al. decorating the surface of a magnetic coating could exhibit surface plasmon resonance. Based on my work in the field and understanding of the physical phenomena of surface plasmon resonance (SPR), I submit that the structure of Filas et al. with silicon nanowire having a magnetic coating decorated with nanoscale metal particles on the surface of the magnetic coating eliminates surface plasmon resonance in the nanoparticles. I base my conclusion that Filas et al. cannot support surface plasmon resonance in the nanoparticles coated thereon for the reasons detailed in Paragraphs 6-9.

6. At Column 11, Lines 1-15, Filas et al. teach mixing of nano-scale nanoparticles of metal or metal precursor into the liquid carrier **32** (water or solvent) containing the magnetic-coated nanowires **34** as shown in Fig. 2A. The particle size is in the range of 1-1000 nm, advantegously in the range of 2-50 nm. For Ag, Cu, Co, and Au nanoparticles, surface plasmon resonance is rapidly lost as particle size increases above 100 nm [U. Kreibig and M. Vollmer, "Optical Properties of Metal Clusters," Springer, New York (1995)]. Therefore, for surface plasmon resonance considerations, the required particles size is within 100 nm. In this size range, the particles are also suspended in water or solvent by the available thermal energy at room temperature, if they are monodispersed. On the other hand, as Filas et al. further teaches in the next paragraph, Column 11, Lines 16-30, the precursor nanoparticles **30** are allowed to settle, as shown in Fig. 2B. Based upon the common knowledge in the literature [U. Kreibig and M. Vollmer, "Optical Properties of Metal Clusters," Springer, New York (1995)], such "settling" of nanoparticles in a solvent can only occur if the particles form aggregates, which are then too heavy to be suspended by thermal energy. Subsequently, the aggregates form a "consolidated matrix" surrounding the magnetic-coated nanowires as shown in Fig. 2B. The resultant "composite" is then dried into a solid body. Finally, the surface of the composite is exposed to

an etching process to allow the nanowires to protrude. Obviously, this structure taught by Filas et al. is very different from what we claim in our invention. First, unlike in Filas et al., our nanoparticles are monodisperse and do not form aggregates. The electron microscopy micrographs and optical extinction spectra in our specification are solid evidences for the presence of monodispersed particles. Second, because of the same reason, our particles do not form a consolidated matrix around the nanocolumns or nanowires as taught by Filas et al. In my recognition, the purpose of such consolidated matrix of nanoparticles is structural stabilization (support) of magnetic-coated particles analogous to a concrete foundation constructed from cement and sand. In our invention, the columns are already structurally stable and the role of the nanoparticles is not structural stabilization. Consequently, our particles do not form and do not have to form a consolidated matrix or composite as taught by Filas et al. Such aggregated or consolidated matrix of metal nanoparticles cannot sustain surface plasmon resonance due to electrical (i.e., physical) contact between the nanoparticles. Electron conduction between the metal particles eliminates the surface plasmon resonance once electrons are not bound to a certain nanoparticle and they are not subject to a restoring (confining) imposition. As a result, the nanoparticle structure disclosed by Filas et al. cannot exhibit surface plasmon resonance. In summary, the dissimilarity between the structures claimed by Filas et al. and claimed in our invention has the dramatic consequence of absence versus presence of surface plasmon resonance, respectively.

7. Filas et al. is silent as to whether this magnetic coating constitutes a surface film or nanoscale particulate. By way of background, there are two types of surface plasmons. Localized surface plasmons are what one observes in metal nanoparticles and surface plasmons that travel along the interface between a metallic film and a dielectric. These two types of

plasmons, localized surface plasmons and surface plasmons, are physically very different from one another. Surface plasmons excited on a continuous metal surface only excite continuous metal surfaces and can be excited only at a certain angle of incidence of light due to momentum conservation as well as requiring a specific photon energy. In contrast, localized (nanoparticle) surface plasmons can be excited at any incident direction due to symmetry or relaxation of the momentum conservation. Of note is that localized (nanoparticle) surface plasmons and surface plasmons are capable of interaction such that energy transfer takes place from one to another, which is commonly termed plasmonic coupling.

8. In the instance where magnetic materials applied by Filas et al. form a continuous surface, any metal nanoparticle deposited thereon will not exhibit surface plasmon resonance through interaction of localized plasmonic states of the nanoparticle with a continuous band of plasmonic states associated with the magnetic underlayer. [Avery, the truth is that the plasmon resonance will be modified in energy and width, and will be lost in certain polarizations, but it will not be completely lost]. While unclear from Filas et al., I surmise that the magnetic material must have a degree of continuity, else magnetic field cancellation would result from random orientation decorating particles.

9. I also note that Filas et al. appears to be relied upon for a teaching of uniform dispersion of nanoscale particles of metal on top of this magnetic coating at column 11, lines 1-15. My reading of Filas makes clear to me that exposing magnetic material coated nanowire array to such a solution of premade particles would not achieve particle deposition uniformity due to the high aspect ratio of the nanowires that results in a gradient of particle penetration between the free surface of the nanowires and the base thereof that results in either a relative deficiency of particles at the base of the nanowires in instances when synthesized particles tend

to adhere upon contact with the metallic coated nanowire, or in the alternative, with a weak interaction between the particle and the magnetic coated nanowire that the particles upon drying the solution carrying the particles results in a comparative densified layer of such particles at the base of the nanowires, as appears to be implied in Filas et al. with reference to Figure 2b. As such, Filas et al. is also distinguished from claim 99 in that the metal nanocrystals are not uniformly spaced between the nanowires of the array and instead form particle gradients along the length of the nanowires.

10. I understand that claims 99-102 and 104 are also considered to be obvious over Debe on the basis that Debe teaches a uniform covering of isolated nanocrystals of platinum. I dispute this finding on the basis of the clear language in Debe at column 14 that shadowing caused by the microstructures themselves tends to create a deposition gradient with the tops of the structures relative to the deposition source being coated with a greater amount of material than deeper portions of such structures. This teaching of Debe is consistent with what one observes in vapor deposition processes and indeed limits the aspect ratio of trenched features in semiconductor substrates that can be filled by this technique. Owing to the highly reactive nature of vapor deposition precursors, atoms in the deposition source that contact a substrate tend to have a high propensity to adhere upon the initial contact and as closer surfaces are exposed to more deposition atoms tend to develop growths of deposited material more quickly which further occludes deeper regions from exposure to gaseous deposition atoms. I believe it is inappropriate to cite to Figure 2b of Debe for showing uniform deposition, as the above-referenced section of Debe clearly indicates that preferential growth has occurred in these images and it is further noted that the image in 2b only shows a portion of the microstructures. Consistent with the teachings of Debe and the limited visualized field of Figure 2b, I believe portions of the

nanostructures farther from the deposition source in fact show lower density of deposition thereon. As such, it is unclear to me how Debbie renders obvious claim 99 with respect to metal nanocrystals spaced uniformly between the columns of the array of nanostructured silicon columns.

11. It is my understanding that claims 99 and 101-104 are considered obvious over Sun et al. in view of Zhang et al. I note that the silicon nanowire of Sun et al. is created through a laser ablation technique and is necessarily polycrystalline while that of Zhang et al. is a single crystal. In both the present invention and Sun et al., metal nanopartieles are produced by reduction by simple immersions without the aid of an additional reducing agent, surfactant, or other complexing agents. As the silicon structure serves as the reducing agent, the energetics of the silicon valence band dictate the electron volts available in an electron perform work namely reduction of a metal cation ineorporated into the metal nanocrystal. I note that the half cell reactions in Sun et al. at page 6399, first column, appear to me to be correct. However, these half cell reactions while operative for a polycrystalline system do not take into aecount the different surface energetics and reactivities of various silicon faces. Provided herewith is a general referenee that shows the different surface energetics for common faces of hydrogen terminated silieon. [J. M. Lysko, "Anisotropic etching of the silicon crystal-surface free energy model," Materials Scienee in Semiconductor Proeessing, vol. 6, pp. 235-241, 2003.] This difference in surface face energetics has implications in the event that one attempts to use a silicon nanocrystal nanowire as a reducing agent in that reduction and therefore nanoparticle growth are known to occur preferentially on low energy silicon surfaees relative to the high energy surfaces. As sueh, substitution of the single crystal silicon nanowire of Zhang et al. for that of Sun et al. would be expected not to produce a uniform spacing of metallic nanocrystals on

the nanowires, but rather a preferential distribution based on silicon nanowire facets. As a result, I believe that the combination of the silicon nanowire of Zhang et al. and the process of Sun et al. would not afford the claimed invention.

12. I declare that all statements made herein of my own knowledge are true and that all statements made on belief and information are believed to be true. These statements are made with the knowledge that willful false statements and the like so made are punishable by fine or imprisonment, or both, under Section 1001 of Title 18 of the United States Code, and that such willful false statements may jeopardize the validity of the application or any patent issuing thereon.

Dated: December 26, 2009 /Ali Kaan Kalkan/
Ali Kaan Kalkan

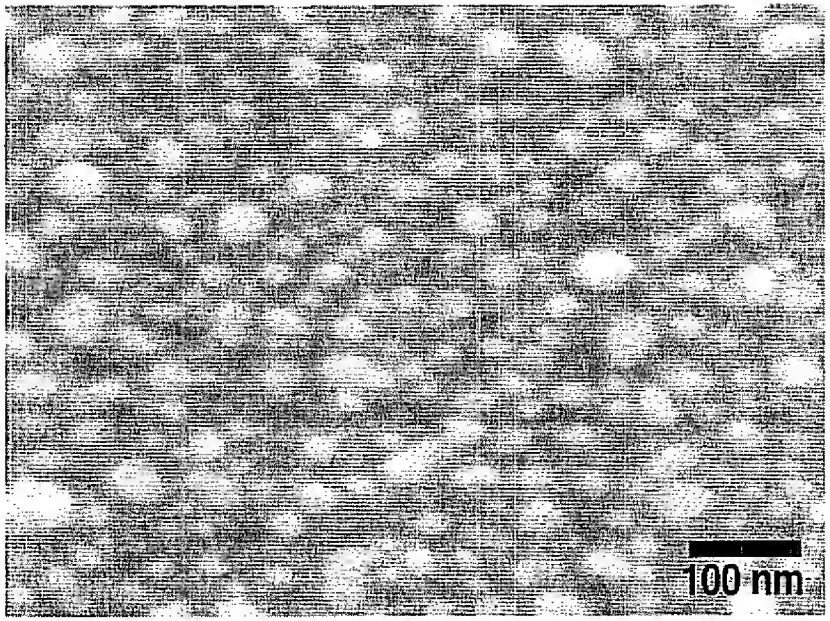
100 nm

Available online at www.sciencedirect.com
SCIENCE DIRECT®
PERGAMON
Materials Science in Semiconductor Processing 6 (2003) 235–241
MATERIALS SCIENCE IN SEMICONDUCTOR PROCESSING

Anisotropic etching of the silicon crystal-surface free energy model

Jan M. Łysko*,[1]

Institute of Electron Technology, Al. Lotników 32/46, 02-668 Warsaw, Poland

Abstract

Mechanism of the silicon crystal wet chemical etching is still debated. Some aspects related with the fast etching convex corners are not yet completely understood and explained by the birth-and-spread mechanism. Simple model based on the new physical hypothesis consisting two independent mechanisms is proposed. The first one is related to the electrostatic charge presence at the sample interface. This charge is supposed to be responsible for the Si–Si bonds simultaneous breaking in the specific locations of the crystal lattice and the whole mono atom layer (or several layers) release to the etching solution. Etching vector associated with this mechanism is vertically oriented to the sample surface. Second mechanism of the model has etching vector laterally oriented to the (1 1 1) crystal plane and applies to the rough crystal surfaces and to the crystal planes other than (1 0 0) and (1 1 1). In the model atoms which are highly exposed to the etching solution over the sample surface have lower activation energy and are etched off with much higher rates than with the vertical vector mechanism. This can be observed as a rough surface planarization and crystal surface quality improvement with the etching progress. Anisotropic etching model deals with the two stable silicon crystal planes (1 1 1) and (1 0 0), and five semi-stable crystal planes (1 1 0), (1 1 2), (1 1 3), (2 2 1), (3 3 1), which are present at the sample face, during the convex corner mask etching.

Keywords: Silicon; Crystal; Anisotropy; Etching; Model

1. Alkaline anisotropic etching solutions

The most popular non-organic solutions applied for the silicon crystal anisotropic etchings are alkaline hydroxides: KOH [1–10], NaOH [5,8,10,11], LiOH [5,6,8], CsOH [5,8,12], RbOH [8]. The first applied organic etching medium was hydrazine NH_2–NH_2 with the pyrocatechol $C_6H_4(OH)_2$ addition (advantageous but not necessary) [5,10]. Highly toxic and instable hydrazine can be replaced by the EDP (ethylene diamine + pyrocatechol, NH_2–CH_2–CH_2–NH_2) [5,6, 10,13] and its derivatives NH_2–CH_2–CH_2–CH_2–NH_2, NH_2–CH_2–CH_2–CH_2–NH_2, NH_2–$(CH_2)_6$–NH_2 [5], as well as the choline $(CH_3)_3N(CH_2CH_2OH)OH$ [5]. There are some signals about possible ammonium hydroxide NH_4OH applications [5,14], too. At present, TMAH (tetra methyl ammonium hydroxide and water, $N(CH_3)_4OH + H_2O$) is the most frequently reported as an anisotropic etching solution, convenient and compatible to the silicon-advanced technology [1,5,15–20]. Alcohol (ethyl, IPA) addition to the most alkaline solutions acts as a chemical reaction moderator. With the certain mixture proportions improvement of the silicon crystal surface smoothness can be observed as well. Light, temperature and other forms of energy delivered to the etching system strongly affect the etch rate and index of anisotropy. Even pure water, subjected to the microwaves treatment reveals chemical activity as the alkaline solution [4]. Etching process can be slowed down, or even stopped, with application of the heavily doped layer (chemical etch-stop) [10]. External electrical polarization of the lightly doped layers acts in the

*Fax: +48-22-847-15-51.
E-mail address: jmlysko@ite.waw.pl (J.M. Łysko).
[1] SM IEEE.

1369-8001/$ - see front matter © 2003 Elsevier Ltd. All rights reserved.
doi:10.1016/j.mssp.2003.09.003

similar way and one can apply it for precise control of the etch depth (electrochemical etch-stop) [17,19,21,22].

Several publications deal with the process modeling, simulation and software design tools useful for the anticipation of etched crystal profile [1,12,23,24]. The mechanism of the wet chemical etching of silicon crystal is still debated, while some aspects as (e.g. emergence of quasi-stable crystal planes in the fast etching convex corners regions) are not yet completely understood [25]. Scanning tunneling microphotographs (STM) presented by Allongue et al. [26,27] revealed presence of the mono-atomic layer terraces 0.31 nm high, several tens of nm wide, after the silicon etching in the different NaOH solutions. Samples used in these experiments were Si(1 1 1) wafers with the 0.7° miscut angle in the [1 1 $\bar{2}$] crystal direction. This observation brought many researches to the conclusion, that anisotropic etching of the silicon crystal can be explained by the two mechanisms: nucleation of the mono-layer etch pits and successive spread out with the step motion on the surface. This mechanism is also called the "birth-and-spread" [25]. One should consider that birth-and-spread mechanism should strongly depend on the vacancy and dislocation density in the silicon crystal, as well as the samples presented in [26,27] were obtained without the mask application and mask edge presence, which should stop new terraces formation.

2. Silicon crystal properties

Elementary silicon crystal cell consists of eight atoms connected together by 16 covalent bonds. They are arranged in the regular diamond structure of *Fd3m* class of symmetry. Energy required to separate single atom from the crystal lattice is 4.63 eV (106.7 and 446 kJ/mol), at assumed temperature of 0 K and pressure of 1 atm [28]. This means, that the energy required to break single covalent bond Si–Si is twice less, 2.315 eV. This value is much higher than the activation energy calculated by Seidel et al. [5], for different alkaline etching solutions, concentrations and temperatures.

Standard "ball and stick" model was applied for the geometrical analysis. Elementary silicon crystal cell with the side length of $a_{Si} = 0.543$ nm, with the balls of $r = 0.1175$ nm radius representing silicon atoms, and sticks of $l = 0.235$ nm length representing Si–Si covalent bonds, was multiplied into the $5 \times 5 \times 5$ cube (75 elementary cells in the model). Selection of only seven crystal planes: (1 1 1), (0 0 1), (1 1 0), (1 1 2), (1 1 3), (2 2 1), (3 3 1), resulted from the experimental work done with the convex corner mask etching [3,17,12]. These planes are called "semi-stable" because they change shape and after sufficiently long time completely vanish from the sample profile in anisotropic solution. Cube was one-by-one intersected by these planes. All the atoms and bonds located above the plane were removed from the computer graph. This allowed convenient observations of the silicon crystal surface in the 3D configuration, with color, rotation and magnification software options. Ball and stick model was also useful for the surface density calculations of the atoms and bonds for each selected crystal plane. General crystallographic principles, identical to those, applied for the atoms number definition in the elementary crystal cell, were applied: atoms/bonds inside the selected, repetitive, rectangle area were added to the number of corner atoms/bonds (divided by 4), and to the number of side atoms/bonds (divided by 2). Results of these calculations are summarized in Table 1 and compared with the Hesketh et al. data [12]. Significant differences were found for the (2 2 1) and (3 3 1) planes.

3. Etch rate and surface quality

Surface free energy model is based on the experimental etch rate measurements and surface quality observations, in relation to the crystal orientation, type of the alkaline solution and other process parameters. Experiments were done with the KOH, KOH + IPA,

Table 1
Free bonds surface density compared to the published data, relative chemical activity coefficient, angles between the (*h k l*) and (1 1 1) crystal planes

Silicon crystal plane (*h k l*)	Free bonds surface density $\beta_{(hkl)}$		Angle with plane (1 1 1)		
	(nm^{-2})	($\times 10^{15}/cm^2$) [12]	α_{hkl} [29]	$\sin(\alpha_{hkl})$	
(1 1 1)	7.83	0.78	—	—	Fig. 2
(2 2 1)	9.04	1.36	15°48′	0.2723	Figs. 3 and 4
(3 3 1)	9.34	1.17	16°50′	0.2896	Fig. 5
(1 1 0)	9.59	0.96	35°16′	0.5774	Fig. 6
(1 1 2)	11.08	1.11	19°28′	0.3333	Fig. 7
(1 1 3)	12.27	1.23	29°30′	0.4924	Fig. 8
(0 0 1)	13.57	1.36	—	—	Fig. 9

TMAH and TMAH+IPA alkaline solutions. Micrographs from the scanning electron microscope were used to compare roughness of the stable crystal planes (1 0 0), (1 1 1), and semi-stable planes (1 1 0), (1 1 2), (1 1 3), (2 2 1), (3 3 1) of the etched sample profile.

Classic KOH+water solution gives the highest etch rate in every crystallographic direction, the highest index of anisotropy ($V_{[1\,0\,0]}/V_{[1\,1\,1]} = 400/1$ [10]) and the best surface quality. Few percent IPA addition can be applied to moderate chemical reaction and to improve temperature stability of the etching solution. Only few percent of weight—because of the low KOH/IPA solubility. The boiling point of IPA is around the 82°C. Its excessive content over the solubility level evaporates and circulates in the etching system: from the solution, through the reflux condenser, back to the solution container. It was observed, that IPA addition does not change the etch rate $V_{[1\,0\,0]}$, but significantly reduces the etch rate $V_{[1\,1\,0]}$. This observation indicates, that anisotropic etching consists of at least two mechanisms, and these mechanisms can be individually controlled by the chemical composition of etching solution.

IPA addition to the etching solution of low KOH concentration deteriorates the (1 0 0) crystal plane quality. Worse substrates and products circulation from/to the silicon-solution interface to/from the free electrolyte volume was supposed to cause poor surface smoothness with scattered pyramid structures located in the regions close to the concave corners of the masking layer. Pyramid formation process can be compensated by the higher KOH concentrations.

TMAH etching solutions seems to be advantageous over the KOH because of their good compatibility with the standard IC CMOS technology. TMAH is widely applied as a component of positive resist developer. It is chemically stable up to 130°C, non-volatile, non-toxic and less destructive to the metal elements. These properties are very useful for the technology designers. In comparison to the KOH, the etch rate and index of anisotropy are lower, but still satisfactory for the MEMS technology. Generally, in the TMAH+water solutions silicon crystal etch rate in every direction decrease with the mixture concentration. Experimental characteristics are almost linear. For example, in the [1 0 0] crystal direction and temperature close to the 80°C, the etch rate changes from 0.9 μm/min in 5% TMAH, to 0.5 μm/min in 30% TMAH. Application of etching solutions with high TMAH concentrations (above 13 pH) is not recommended because of increased possibility of hillock formation on the (1 0 0) crystal planes.

IPA addition to TMAH+water solution also moderates chemical activity and improves crystal surface smoothness. Concentration of TMAH and IPA strongly, but not in the constant proportion, affects crystal etch rates in different crystal directions. This observation also brings to the suggestion that anisotropic etching process consists of at least two independent etching mechanisms. They have different electrochemical nature and different impact on the total etch rate, depending on the process parameters.

4. Vertical etch rate vector

In the model electrostatic charges at the silicon-solution interface are responsible for the crystal anisotropic etching with the vertical etch rate vector. Crystal surface consists of the silicon atoms with one (Si^{+}), two (Si^{2+}), or even three (Si^{3+}) active bonds directed to the surrounding medium. At the room temperature and in the air, these bonds capture electrons from the ambient oxygen atoms and form so-called "native oxide", several angstroms thick. In the alkaline solutions, these active bonds represent positive charges at the sample surface, which induce electrostatic field. This field is proportional to the active bonds number (Table 1) and affects both sides of the interface: etching solution and silicon crystal lattice. In the etching solution, close to the interface, Helmholtz zone rich of OH^- ions is induced (Fig. 1) [30]. From the silicon crystal side, electron-enhanced zone deflects valence and conduction bands of the semiconductor [28].

Valence single electron e ($=-1.6\times10^{-19}$ C) of the silicon atom in the crystal lattice, separated by the distance d ($=0.543$ nm, silicon elementary cell constant) from the single, positive elementary charge $q = -e(=+1.6\times10^{-19}$ C) located at the interface, with the

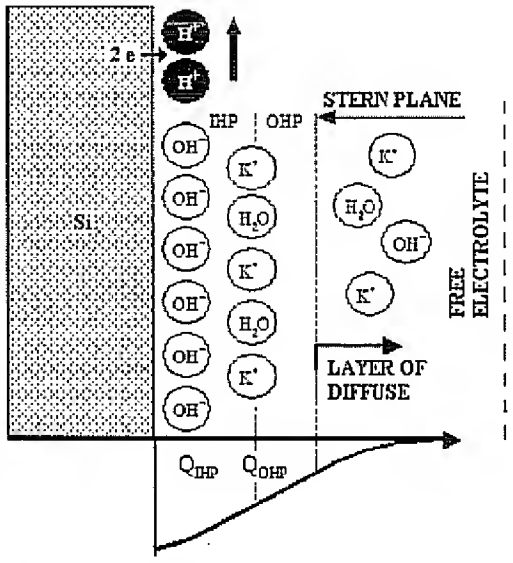

Fig. 1. Electrostatic charge distribution scheme at the Si–KOH interface; IHP—Internal Helmholtz Plane, OHP - Outer Helmholtz Plane, Q - electrostatic charge [30].

dielectric vacuum constant ε_0 assumption, has potential energy estimated by

$$U = \frac{eq}{4\pi\varepsilon_0 d} \approx 2.65\,\text{eV}. \quad (1)$$

One should notice, that this value is higher than the average Si–Si break bond energy (2.15 eV).

It was assumed that stable crystal planes (1 0 0) and (1 1 1) are etched in the model with the vertical vector only. Atom arrangement at the silicon crystal (1 1 1) plane is the tightest one. There is only one free covalent bond per atom at the interface which results in low surface bonds density $\beta_{(1\,1\,1)}$ (= 7.83 bonds/nm^2, Table 1, Fig. 2). Other three bonds of each atom are involved in the inter-layer integrity. This layer is attached to the crystal bulk with the only one bond per atom (weak spots of the lattice) and supposed in the model to be responsible for the anisotropy phenomenon. Electrostatic field at the interface seems to be sufficiently high to break these weak bonds and whole atom layer peel from the crystal bulk. With the etch rate of 0.5 μm/min about 4000 atom layers per minute are transferred to the liquid, where the crystal lattice decomposition is finished. Similar etching mechanism apply to the (0 0 1) crystal plane (Fig. 9). The only difference is less tight arrangement of silicon atoms and higher free bonds surface density $\beta_{(0\,0\,1)}$ (= 13.57 bonds/nm^2, Table 1). Semi-stable crystal planes (1 1 0), (1 1 2), (1 1 3), (2 2 1), (3 3 1) selected for the model considerations, etch in the alkaline solutions both with vertical and lateral etching vectors.

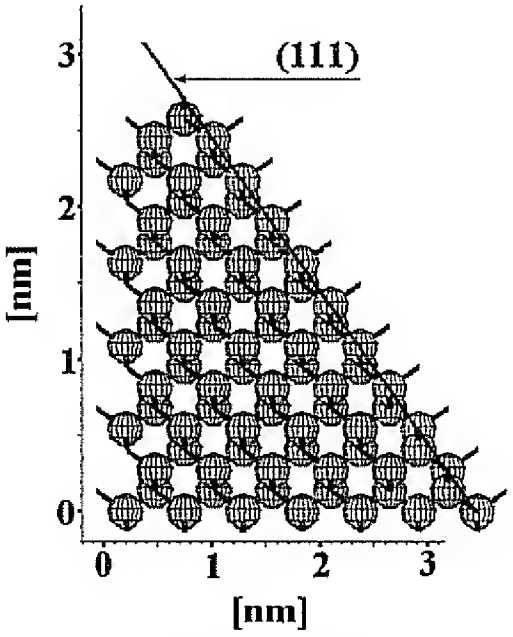

Fig. 2. Atom arrangement on the (1 1 1) silicon crystal plane, ($\upsilon = -45°$, $\varphi = 90°$).

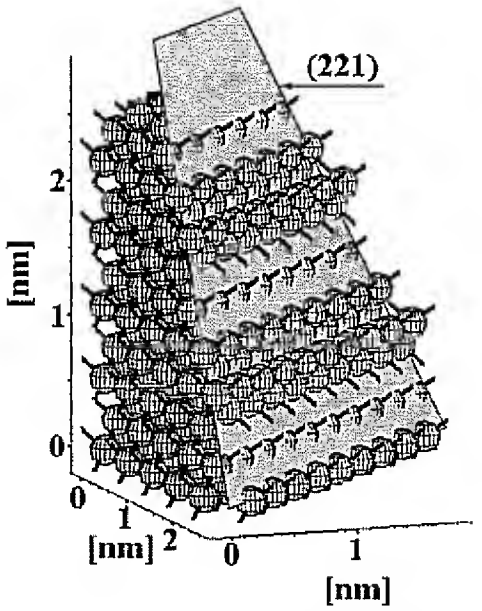

Fig. 3. Atom arrangement on the (2 2 1) silicon crystal plane, ($\upsilon = -20°$, $\varphi = 80°$).

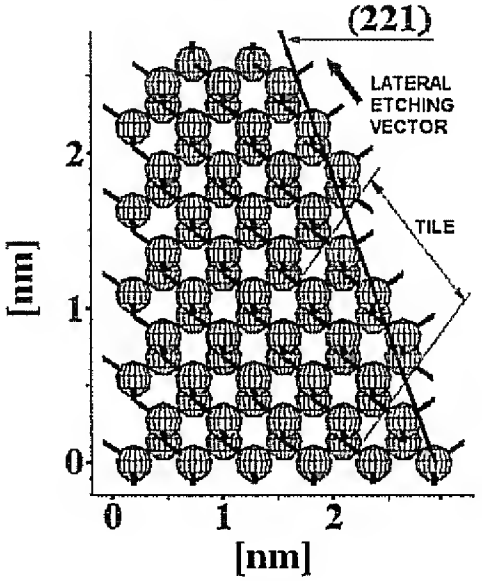

Fig. 4. Atom arrangement on the (2 2 1) silicon crystal plane, ($\upsilon = -45°$, $\varphi = 90°$).

5. Lateral etch rate vector

Model of the silicon semi-stable crystal planes anisotropic etching consists of the mechanism, similar to the birth-and-spread and etch pits spread out with the mono-atomic layer step motion on the surface [25]. It has a very strong impact on the total etch rates of rough surfaces, as well as in the crystal directions under consideration: [1 1 0], [1 1 2], [1 1 3], [2 2 1], [3 3 1]. Lateral

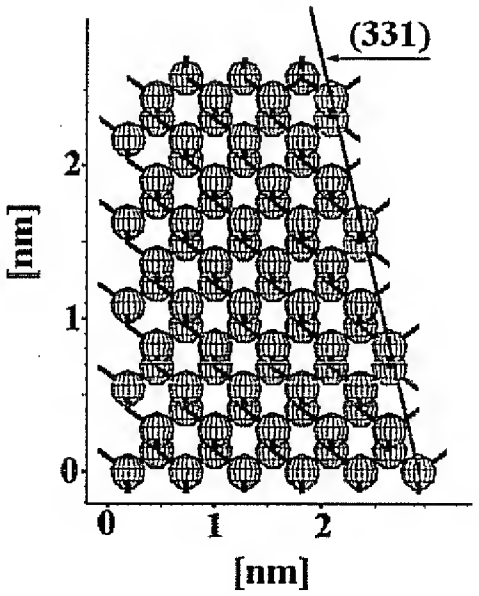

Fig. 5. Atom arrangement on the (3 3 1) silicon crystal plane, ($\upsilon = -45°$, $\varphi = 90°$).

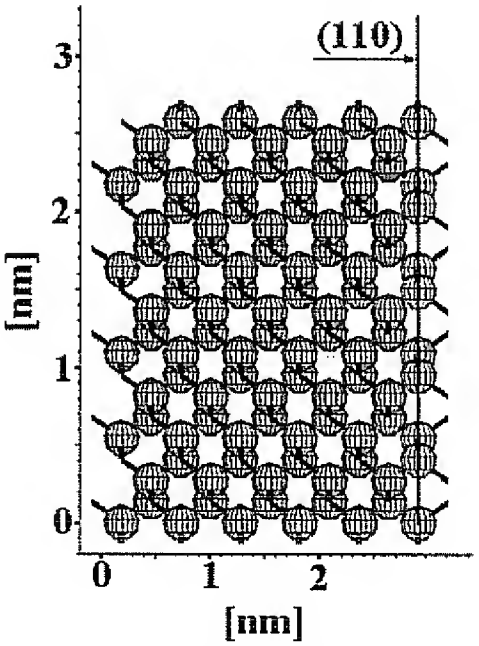

Fig. 6. Atom arrangement on the (1 1 0) silicon crystal plane, ($\upsilon = -45°$, $\varphi = 90°$).

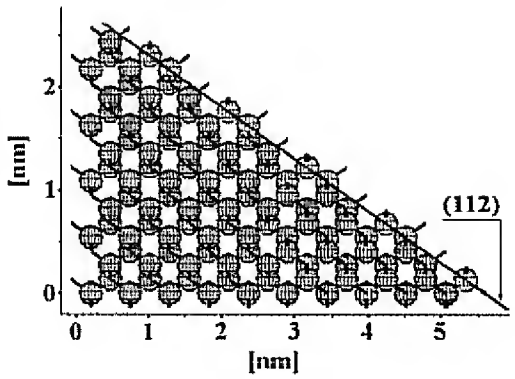

Fig. 7. Atom arrangement on the (1 1 2) silicon crystal plane, ($\upsilon = -45°$, $\varphi = 90°$).

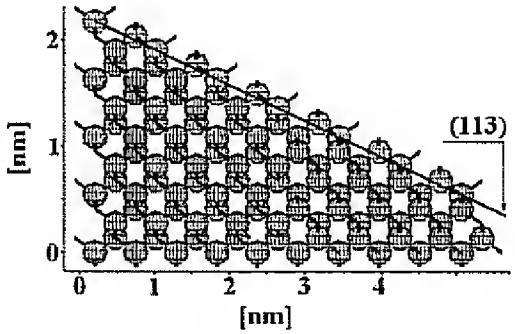

Fig. 8. Atom arrangement on the (1 1 3) silicon crystal plane, ($\upsilon = -45°$, $\varphi = 90°$).

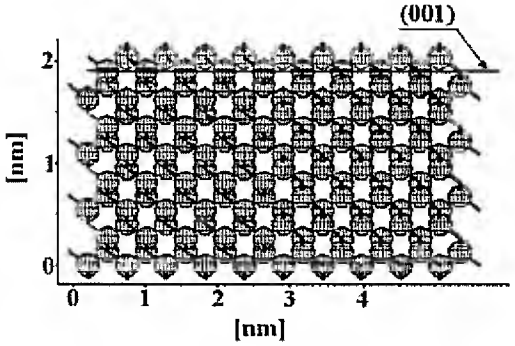

Fig. 9. Atom arrangement on the (0 0 1) silicon crystal plane, ($\upsilon = -45°$, $\varphi = 90°$).

etch rate vector, parallel to the (1 1 1) crystal plane is high and results in the surface planarization and final smoothness improvement. After sufficiently long time all the unevenness and semi-stable planes should progressively vanish to the only (1 1 1) and (1 0 0) crystal planes. In the model, lateral etching vector module was assumed to be identical for the all semi-stable crystal planes. This assumption comes from the identical atom arrangement in parallel to the (1 1 1) crystal plane.

Ball and stick model allows observation of the surface and bulk atom arrangement with slope υ and φ. At the etched interfaces atoms are arranged in the tile-like configuration, with one (1 1 1) atom layer overlapping another (1 1 1) atom layer located under the first one.

Tiles of (2 2 1) and (1 1 2) planes (Figs. 4 and 7) consist of 5-atom clusters in row crystal orientation [1 $\bar{1}$ 0], with the free bonds oriented to the etching solution. Tile of (3 3 1) plane (Fig. 5) consists of 4-atom cluster, tile of (1 1 3) plane (Fig. 8) consist of 3-atom cluster, and tile of (1 1 0) plane (Fig. 6) is the shortest one, and consist of only 2-atom cluster.

Exposition angle of atoms at the layer step is very wide (250°). Steps are parallel to the [1 $\bar{1}$ 0] crystal direction, with the mirror plane (1 $\bar{1}$ 0) of symmetry. There are also empty channels 0.17 nm wide and 0.17 nm high, visible in the ball and stick model from the [1 $\bar{1}$ 0] crystal direction. These channels connect octaedric gaps inside every elementary silicon crystal cell. Theoretically, atoms located at the layer steps are supposed to have identical electrochemical potential and should be etched simultaneously with the same etch rate. Non-perfect conditions should be considered in anisptropic etching model with the lateral vector: mixture stirring intensity, temperature distribution over the sample surface, location of the atom tiles in respect to the mask edges, as well as the interface aspect ratiochanges. These circumstances can explain observed worse smoothness of the semi-stable crystal planes after the anisotropic etching (randomly stepped), widely reported and illustrated with SEM micrographs in [1–3,23,12].

6. Model of anisotropic silicon crystal etching

In the model total etch rate of the crystal can be expressed by the following expression:

$$V \sim V_V + V_L \tag{2}$$

where V_V represents the etch rate of vertical vector associated with the electrostatic field, and V_L represents the etch rate of lateral (1 1 1) plane vector. First component was assumed to be an exponential function, with the bonds density $\beta_{(hkl)}$ proportional to the average chemical activity of the atoms at the crystal planc $(h\,k\,l)$. Bonds density change from one crystal plane to another in the non-linear, non-monotonic way, according to the atoms/bonds lattice arrangement.

$$V_V \sim \exp(\beta_{(hkl)}). \tag{3}$$

Second component has collinear trigonometric point characteristic and non-monotonic nature:

$$V_L \sim \sin(\alpha_{(hkl)}), \tag{4}$$

where $\alpha_{(hkl)}$ represents (hkl)-to-(1 1 1) angle. $\beta_{(hkl)}$, $\alpha_{(hkl)}$ and $\sin(\alpha_{(hkl)})$ are enclosed in Table 1.

7. Parameters extraction

Model has only two constants A, B to be extracted from the experiment:

$$V = A\exp(\beta_{(hkl)}) + B\sin(\alpha_{(hkl)}). \tag{5}$$

For the given KOH + H_2O 10 M solution, at 80°C, measured etch rates are $V_{[3\,1\,1]} = 1.9\,\mu m/min$ and $V_{[1\,0\,0]} = 0.9\,\mu m/min$ [1]. Index of anisotropy is $V_{[1\,0\,0]}/V_{[1\,1\,1]} = 400:1$ [10]. This means, that the etch rate in the [1 1 1] direction is $V_{[1\,1\,1]} = 0.00225\,\mu m/min$. These data allow estimation of the model constants from Eq. (5). For the given process conditions Eq. (2) constants are: $A = 0.8947 \times 10^{-6}$, $B = 3.4713$, and calculated etch rates in reminding crystal directions are:

$$\begin{aligned}
&V_{[hkl]} = A\exp(\beta_{(hkl)}) + B\sin(\alpha_{(hkl)})\\
&V^*_{[1\,1\,1]} = 0.00225 + 0 = 0.00225\,\mu m/min\\
&V_{[2\,2\,1]} = 0.00756 + 0.94523 = 0.95279\,\mu m/min\\
&V_{[3\,3\,1]} = 0.01019 + 1.00529 = 1.01548\,\mu m/min\\
&V_{[1\,1\,0]} = 0.01308 + 2.00433 = 2.01741\,\mu m/min\\
&V_{[1\,1\,2]} = 0.05803 + 1.15698 = 1.21501\,\mu m/min\\
&V^*_{[1\,1\,3]} = 0.19075 + 1.70927 = 1.90002\,\mu m/min\\
&V_{[0\,0\,1]} = 0.69993 + 0 = 0.69993\,\mu m/min\\
&{}^*\text{these directions were used to extract } A,\ B \text{ constants}\\
&\text{for the model.}
\end{aligned} \tag{6}$$

These results are consistent with the experimental ones. Etch rate order in the given process conditions is: $V_{[1\,1\,1]} < V_{[0\,0\,1]} < V_{[2\,2\,1]} < V_{[3\,3\,1]} < V_{[1\,1\,2]} < V_{[1\,1\,3]} < V_{[1\,1\,0]}$. Model enables calculations of the silicon crystal etch rates for another high index directions and process conditions.

8. Discussion

Coulomb potential shielding of the electrostatic field should be considered in the model optimization, particularly in the vertical etch rate vector mechanism. Electron energy from estimation (1) should be reduced by factor λ representing potential shielding range [28]:

$$\frac{1}{\lambda} \sim \left(\frac{E_F}{6\pi n_0 e^2}\right)^{1/2}, \tag{7}$$

where E_F is the electron Fermi energy level and n_0 is the electron concentration. With this expression the etch-stop (on the highly doped layer or externally polarized junction) can be explained. Shielding range depends on the atoms arrangement and crystal orientation of the crystal interface, so it should be denoted as $\lambda_{(hkl)}$. It is expected to be much higher for the (1 1 1) crystal plane because of the highest atom density, than for the (1 0 0) crystal plane.

Presented model of the silicon crystal anisotropic etching consists of two independent mechanisms. Two etching vectors have been distinguished—one vertical to the crystal-solution interface and second parallel to the (1 1 1) crystal plane. With the model, worse smoothness of the semi-stable silicon crystal planes and almost perfect atomic smoothness of the (1 1 1) and (1 0 0) planes after the alkaline solution etching can be explained. Electrostatic field presence at the silicon crystal-solution interface, its interaction with the remote covalent Si–Si bonds in the crystal lattice, low number of Si–Si covalent bonds between the atomic crystal planes (weak lattice spots), as well as the strong in-plane bonds structure, are supposed to be responsible for the anisotropic etching phenomenon.

References

[1] Zubel I. Sens Actuat 2001;A94:76.
[2] Zubel I. Sens Actuat 2000;A84:116.
[3] Barycka I, Zubel I. Sens Actuat 1995;A48:229.
[4] Dziuban JA. Proc Eurosensors XIII Conf 1999;18B4:671.
[5] Seidel H, Csepregi L, Heuberger A, Baumgärtel H. J Electrochem Soc 1990;137:3612.
[6] Seidel H, Csepregi L, Heuberger A, Baumgärtel H. J Electrochem Soc 1990;137:3626.
[7] Smith L, Söderbärg A. J Electrochem Soc 1993;140:271.
[8] Wang T, Surve S, Hesketh PJ. J Electrochem Soc 1994;141:2493.
[9] Petit B, Pelletier J, Molins R. J Electrochem Soc 1985;132:982.
[10] Petersen KE. In: Muller RS, Howe RG, Senturia SD, Smith RL, White RM, editors. Microsensors. New York: IEEE Press; 1991. p. 39.
[11] Rappich J, Lewerenz HJ, Gerischer H. J Electrochem Soc 1993;140:L187.
[12] Hesketh PJ, Gowda CJuS, Zanoria E, Danyluk S. J Electrochem Soc 1993;140:1080.
[13] Finne RM, Klein DL. J Electrochem Soc 1967; 114:965.
[14] Chen L-C, Chen M, Tsaur T-H, Lien C, Wan C-C. Sens Actuat, 1995;A49:115.
[15] Sarro PM, Brida D, Vlist Wvd, Pignatel G, Brida S. Proc Eurosensors XIII Conf 1999;12B4:389.
[16] Voipio V, Nera K, Ruokonen K, Lamminmäki T, Tittonen I. Proc Eurosensors XIII Conf 1999;27B2: 1025.
[17] Tabata O, Asahi R, Funabashi H, Sugiyama S. Proc Transducers'91 Conf 1991; 811.
[18] Schnakenberg U, Benecke W, Lange P. Proc Transducers'91 Conf 1991; 815.
[19] Acero MC, Esteve J, Burrer Chr, Götz A. Sens Actuat 1995;A46–47:22.
[20] Merlos A, Acero M, Bao MH, Bausells J, Esteve J. Sens Actuat 1993;A37–38:737.
[21] Kloeck B, Collins SD, de Rooji NF, Smith RL. IEEE Trans Electron Devices 1989;36:663.
[22] Schmidt B, von Borany J, Todt U, Erlebach A. Sens Actuat 1994;A41–42:689.
[23] Horn A, Wachutka G. Proceedings of the Eigth International Conference on MIXDES, 2001. p. 413.
[24] Séquin CH. Sens Actuat 1992;A-34:225.
[25] van Veenendaal E, Nijdam AJ, van Suchtelen J, Sato K, Gardeniers JGE, van Enckevort WJP, Elwenspoek M. Sens Actuat 2000;84:324–9.
[26] Allongue P, Costa-Kieling V, Gerischer H. J Electrochem Soc 1993;140:1018.
[27] Allongue P, Costa-Kieling V, Gerischer H. J Electrochem Soc 1993;140:1009.
[28] Kittel C. Introduction to solid state physics. New York: Wiley; 1966.
[29] Kelly A, Groves GW. Crystallography and crystal defects. London Group Ltd. ed., 1970.
[30] Lorne B, Perrier F, Avouac JP. J Geophys Res 1999; 104B8:17857.